Change in the elemental composition and cell geometry of the marine diatom *Attheya longicornis* under nitrogen- and iron-depleted conditions

Koji Sugie[1, 2*] and Kenshi Kuma[1, 3]

[1]: Graduate School of Environmental Science, Hokkaido University, Kita 10-Nishi 5, Kita-ku, Sapporo, Hokkaido 060-0810, Japan

[2]: Present address: Research and Development Center for Global Change, Japan Agency for Marine-Earth Science and Technology, 2-15, Natsushima-cho, Yokosuka, Kanagawa, 233-0061, Japan

[3]: Faculty of Fisheries Science, Hokkaido University, 3-1-1 Minato-cho, Hakodate, Hokkaido 041-8611, Japan

*: Author for correspondence

Koji Sugie (sugie@jamstec.go.jp)

Research and Development Center for Global Change, Japan Agency for Marine-Earth Science and Technology, 2-15, Natsushima-cho, Yokosuka, Kanagawa, 233-0061, Japan

Tel: +81-46-867-9449, Fax: +81-46-867-9455

ABSTRACT

The morphology of the siliceous cell wall (frustule) is fundamental to the identification of diatom species. One of the fundamental questions is the ecophysiological role of the diatom frustule, which often shows morphological plasticity under different growth conditions. In this study, the morphology and elemental composition of the diatom *Attheya longicornis* were investigated under nutrient-replete (control), iron-depleted and nitrogen-depleted conditions. This cylindrical, unicellular species has four siliceous horns per cell. The horns are each formed from a hoop-like structure with a supporting rod, which greatly increases the surface area of the cell. Under the iron-depleted conditions, relative to the controls the surface area to cell volume ratio, silicon cell quota, and siliceous horn length increased 2.3-, 2.3- and 1.4-fold, respectively. Under the nitrogen-depleted conditions, the cell size decreased without an increase in horn length, and the cellular biogenic silica content was the highest between the three growth media. The change in cell geometry and elemental composition modified the sinking behaviour of *A. longicornis*. Estimated sinking rate was fastest in the nitrogen-depleted cells, followed by the controls and iron-depleted cells. The data suggest that the biogeochemical processes of biogenic silica could show vertically opposite direction depending on the growth-limiting factors through a change in the elemental composition and cell morphology of diatoms. Such plastic responses to nitrogen and iron depletion may contribute to the relatively wide distribution of this species from the coastal to open ocean in the subarctic region.

Key index words:

diatom; frustule ultrastructure; iron availability; morphological plasticity; nitrogen depletion; sinking rate

Running head: Trade-offs between sinking and silicification

Introduction

Diatoms contribute to approximately 20% of the Earth's oxygen production (Falkowski et al. 1998) and their organic constituents can potentially sink rapidly below the mixed layer depth depending on their relatively large cell size and heavy siliceous cell wall (frustule). Therefore, diatoms drive a substantial part of the biological carbon pump (Smetacek 1999, De La Rocha et al. 2008). After diatom-dominated blooms, sedimentation of their aggregates is a well-known phenomenon (Smetacek 1985). Although frustules are inclined to sink, frustules with eccentric morphologies, especially species with small cells, are thought to resist sinking as the deviation from a sphere increases the surface area to volume ratio (Margalef 1997, Raven and Waite 2004). Previous studies have mainly focused on the relationship between species-specific sinking rates and physiological status (Brzezinski & Nelson 1988, Waite et al. 1992). A change in physiological status under macronutrient- and micronutrient-limited conditions often induces the change in diatom morphology (Sugie & Kuma 2008, Marchetti & Cassar 2009, Wilken et al. 2011, Sugie & Yoshimura 2013). However, testing the effect of morphological variation, frustule morphology and nutritional status in combination is relatively rare.

The morphology of siliceous frustules is used to determine species identity in diatoms. Many species have developed specialized frustule shapes and structures, probably reflecting long-term evolutionary processes (Round et al. 1990, Smetacek 2001, Raven & Waite 2004). Certain diatom groups have spines or horns, some of which have surface ornamentation (Round et al. 1990). These structures should further increase the surface area to volume ratio, presumably reducing sinking to aphotic depths in the open ocean, which is fatal for photosynthetic organisms. By contrast, diatoms that sink in shallow coastal environments may be able to return to the photic layer through mixing events. Therefore, sinking behaviour is one of the important factors affecting phytoplankton dynamics in the ocean (Smetacek 1985, Brzezinski & Nelson 1988, Peperzak et al. 2003). Many coastal diatom species, including their resting spores, increase silicification and sink to deeper waters under micronutrient-replete but macronutrient- or light-limited conditions thereby avoiding grazing and photo-oxidative damage at the surface (Hargraves & French 1983, Raven & Waite 2004, Sugie & Kuma 2008).

In contrast, under micronutrient (iron)-depleted conditions, a diatom cells can increase their surface area to cell volume ratio by changing their cell morphology or extending their siliceous spines, which may regulate sinking velocity (Timmermans et al. 2001, Sugie & Kuma 2008, Sugie & Yoshimura 2013).

The elemental composition of plankton strongly affects the ocean biogeochemical cycling of bioelements (Redfield et al. 1963). A recent study showed that the average nitrogen and phosphate ratios among phytoplankton groups vary and that such variation governs basin-scale variation in seawater nutrient stoichiometry (Weber & Deutsch 2010). Nutrient limitations also affects the cellular nutrient stoichiometry of phytoplankton (Marchetti & Cassar 2009, Sugie & Yoshimura 2013). A deviation in relative nutrient utilization by phytoplankton from the Redfield ratio due to the nutrient limitations could influence the spatial and temporal nutrient availability and therefore productivity (Brzezinski et al. 2002, Sugie et al. 2010b). For example, Sugie et al. (2010a) reported that iron- or nitrate-limited diatoms have high Si:N ratios after the spring bloom peak and that such limitation leads to a decrease in silicic acid availability in the western subarctic Pacific Ocean (Sugie et al. 2010b). Although patterns of limiting nutrients differ spatiotemporally (Tyrrell & Law 1997, Moore et al. 2013), comparisons between the effects of macro- and micro-nutrient limitations on phytoplankton stoichiometry are very limited.

In a steady-state marine ecosystem, macro- or micronutrient limitation often regulates primary productivity (Tyrrell & Law 1997, Moor et al. 2013). Nitrate depletion is often found in the coastal region and subtropical gyres, whereas iron depletion is common in the subarctic Pacific and Southern Ocean (Boyd et al. 2007, Moore et al. 2013). The addition of iron to iron-limited waters could dramatically enhance the growth of phytoplankton, mainly diatoms (Tsuda et al. 2005, Boyd et al. 2007). In this respect, some diatoms should survive under unfavourable, iron-limited conditions in the upper mixed layers. However, previous studies reported that iron limitation could increase diatom silicification (Takeda 1998, Timmermans et al. 2004, Sugie et al. 2010a, Wilken et al. 2011, Sugie & Yoshimura 2013), which may accelerate their sinking rate compared to that of healthy growing cells (De La Rocha et al. 2008, Sugie & Kuma 2008). Plausible mechanisms are still lacking for the survival of diatoms

with heavily silicified frustules at the surface under iron limitation.

We conducted a manipulative experiment using the diatom *Attheya longicornis* R. M. Crawford et C. Gardner under nutrient-replete (control), nitrogen-depleted and iron-depleted conditions to test the effects of the nutritional status of the diatom on its morphology and elemental composition. *Attheya* species have four siliceous horns per cell (23–50 μm in length; Orlova et al. 2002, Stonick et al. 2006), which are composed of hoop-like structures and supporting rods, unlike the setae of *Chaetoceros* species, which have a more or less smooth surface (Round et al. 1990, Crawford et al. 1994). The cylindrical cells are 4–12 μm in diameter and 6–12 μm in height (pervalver length) (Crawford et al. 1994, Orlova et al. 2002, Stonick et al. 2006). Certain *Attheya* species (mainly *A. longicornis* and *A. septentrionalis*) are often found as solitary phytoplankton in the open ocean (Sugie et al. 2010a, Malviya et al. 2016, Sugie and Suzuki in press) or attached by their horns to chain-forming diatoms in the coastal region (Figs 1, 2; Crawford et al. 1994, Orlova et al. 2002, Stonik et al. 2006). The cryophilic species, *A. longicornis*, occurs from subarctic seas to the Arctic Ocean and can survive in darkness for at least several months (Orlova et al. 2002, Sugie et al. 2010a, Tsukazaki et al. 2013). Unravelling the ecophysiology of *A. longicornis* is important to understand their relatively wider distribution in the coastal waters to the open ocean.

Materials and methods

Culture design

The strain of *A. longicornis* used in the experiments was isolated from the western subarctic gyre. The culture was maintained at 10°C under 150 μmol photon m^{-2} s^{-1} fluorescent light (12 h light:12 h dark), using silicic acid-enhanced f/2 medium (Guillard & Ryther 1962). The seawater used for culturing was collected from a coastal region in the northern Japan Sea, near Otaru, Hokkaido Prefecture, Japan. The seawater was filtered using an acid-cleaned 0.22 μm membrane filter (Millipore) and autoclaved for 20 min at 121°C and 108 kPa. The filter was soaked in 1N HCl for at least 24h, followed by repeatedly rinsing and soaking for 24 h with Milli-Q water (>18.0 MΩ cm^{-1}, Millipore). The concentrations of Fe, NO_3+NO_2, NH_3, PO_4 and $Si(OH)_4$ in the autoclaved filtered seawater were less than 2 nmol L^{-1}, 6 μmol L^{-1},

0.1 μmol L^{-1}, 0.4 μmol L^{-1}, and approximately 240 μmol L^{-1}, respectively. The silicic acid-enhanced f/2 medium contained 886 μmol L^{-1} of NO_3, 38 μmol L^{-1} of PO_4 and approximately 350 μmol L^{-1} of $Si(OH)_4$ as macronutrients, and f/2 metals chelated with EDTA. All the macronutrient stock solutions were passed through a Chelex 100 ion-exchange resin to remove trace metals (Morel et al. 1979). Prior to the experiment, the diatom stock cultures were kept in the exponential growth phase for at least 10 doublings by the semi-continuous transfer of cells into the silicic acid-enhanced f/2 medium. Diatoms showing healthy growth were transferred to a modified f/2 medium, prepared without the addition of f/2 trace metals, EDTA, or vitamins. Ferric iron (100 nmol L^{-1}) and manganese (25 nmol L^{-1}) were added to the medium to remove excess trace metals (Sugie & Kuma 2008, Sugie et al. 2010a, 2011). Before the experiment, the algal strain was grown in exponential growth phase for 7 days (or approximately seven cell divisions) in the modified f/2 medium.

Three types of media were prepared for use in the experiment: (1) control, (2) nitrogen (N)-depleted and (3) iron (Fe)-depleted media (Table 1). Silicic acid-enhanced f/2 medium, which was macro- and micronutrient-replete, was used as the control. The N-depleted medium was prepared by adding 5 μmol L^{-1} of NO_3 (instead of 880 μmol L^{-1}) to the silicic acid-enhanced f/2 medium (i.e., 11 μmol L^{-1} of NO_3 in the N-depleted medium). The Fe-depleted medium was prepared by adding 1 μmol L^{-1} of strong iron-binding siderophore desferrioxamine B (DFB) (Sigma Chem. Co. Ltd.) to the modified f/2 medium. In our preliminary experiment, the growth of *A. longicornis* ceased when there was excess DFB relative to ferric iron concentrations, as observed in a previous study using different diatoms (Sugie et al. 2011). Previous studies have demonstrated that the addition of 1 μmol L^{-1} DFB successfully prevents Fe uptake from ambient extracellular Fe by coastal diatoms (Iwade et al. 2006, Yoshida et al. 2006). The culture experiments were conducted in triplicate using acid-washed, polycarbonate 100-mL Erlenmeyer flasks. Manipulations were conducted in a Class 100 laminar flow cabinet to avoid inadvertent contamination.

Measurements

The algal growth was monitored daily using a hemocytometer and a light microscope. Culturing was stopped during the exponential phase for the control samples (day 8), and the

stationary phase for the N-depleted (day 10) and Fe-depleted treatments (day 9). Growth rate (μ, d^{-1}) was determined from the slope of a plot of natural log abundance against time during the exponential growth phase. The Fe and macronutrients were measured by the flow injection method with chemiluminescence detection (Obata et al. 1993) and by continuous flow analysis, respectively (Sugie & Kuma 2008, Sugie & Yoshimura 2013). At the end of the culture period, the cells were harvested for particulate organic carbon (POC), particulate nitrogen (PN), biogenic silica (BSi) and chlorophyll-*a* analysis, as well as for morphometric measurements. For the POC and PN analyses, the samples were passed through a pre-combusted (450°C, 4 h) GF/F filter, and rinsed with 1N HCl-acidified filtered seawater to remove inorganic carbon, and then rinsed with Mill-Q water (> 18.2 MΩ cm^{-1}, Merck KGaA, Darmstadt, Germany). The filter samples for the POC and PN analyses were dried at 60°C overnight and measured using a CHN analyser. For the BSi analysis, the diatom cells were collected on a 0.8 μm pore size polycarbonate membrane filter and rinsed with Milli-Q water to remove silicic acid from the culture medium. The samples were then digested by heating to 85°C for 2 h in a 0.5% Na_2CO_3 solution (Paasche 1980), and the dissolved $Si(OH)_4$ was analysed using a QuAAtro continuous flow analyser. For the chlorophyll-*a* measurements, the culture samples were collected on a GF/F filter and soaked in 6 mL of *N*,*N*-dimethylformamide (DMF) (Suzuki & Ishimaru 1990). The samples were stored at −20°C until analysis. Chlorophyll-*a* was measured using a Turner Design 10-AU fluorometer (Welschmeyer 1994).

Cells of *A. longicornis* were observed using a light microscope and photographed for subsequent size analysis. Measurement of the surface area (SA) and cell volume (CV) of this cylindrical species followed the methods described by Hillebrand et al. (1999). Thus, cell diameter (apical axis) and height (pervalver axis) were measured. Additionally, the length of horns was measured via image analysis with Image-Pro Plus, or using photographs with calibrated scales and a ruler. We measured one fully in focus horn per cell and assumed all horn in a cell were of the same length (Figs 3–5). The measurements were conducted on at least 15 cells per treatment. Horn ultrastructure of the cells grown in the control medium was observed using a scanning electron microscope (SEM). These cells were cleaned with a commercially available alkali-detergent (Pipe Unish: a drain pipe cleaner, S.C. Johnson Inc.),

rinsed with Milli-Q water (Nagumo 1995) and attached to a glass slide. The glass slide was then sputtered with gold prior to examination using the SEM (JSM-6360LA, JEOL Ltd., Tokyo, Japan). Horn (diameter (d_{horn}): 0.51 μm) ultrastructure was measured as the continuum of hoops (or torus) without the supporting rod to simplify the measurements (Fig 3). There were 11–14 (average 12.75, n = 6) hoops per 1.0 μm and their diameter (d_{hoop}) was 0.06 μm. Hoop volume (V_{hoop}) and surface area of the hoop (SA_{hoop}) were calculated using $V_{hoop} = 2\pi^2 \times (d_{horn}/2 - d_{hoop}/2) \times (d_{hoop}/2)^2$ and $SA_{hoop} = 4\pi^2 \times (d_{horn}/2 - d_{hoop}/2) \times d_{hoop}/2$, respectively.

In the present study, the sinking rate of a cell is estimated by Stokes' law as follows:

$$S = g \times R^2 \times (\rho_p - \rho_{sw}) \times 86{,}400 / 18\eta, \quad (1)$$

where S is the sinking rate (m d^{-1}), g is the gravitational acceleration constant (9.8 m s^{-2}), R is the spherical radius of the particle (m), ρ_p and ρ_{sw} represent density (kg m^{-3}) of the particle and seawater, respectively; 86,400 is the number of seconds in a day and η is the dynamic viscosity of seawater (kg m^{-1} s^{-1}). Stokes' law indicates that, where the density of a particle and that of its physical surroundings are the same, the sinking rate increases with the square of the particle radius. Surface area ($4\pi R^2$) to the volume ($4/3\pi R^3$) ratio for a spherical particle increases as its radius (R) decreases, therefore decreasing its sinking rate (S). To estimate sinking rates using Stokes' law, the SA/CV ratios were converted to the corresponding spherical diameter (CSD) of a particle using the following formula: CSD = 6 / (SA/CV). The calculated radius (CSD/2) was substituted into Eq. (1). This simple estimation shows the potential sinking behaviour of a single particle, assuming that the cells do not have a stable position while sinking in a water column.

Statistics

Differences in algal cells between the different culture treatments were tested with Tukey's HSD test, using PASW statistical software (version 17.0 SPSS Inc., Chicago, IL, USA). Significant differences are reported at the 95% confidence level. The data are shown as the means ± 1 standard deviation, each calculated using the results from the three replicate cultures.

Results

Cell growth.

The cells in the control cultures grew exponentially until the end of the experiment (day 8), at a growth rate of $\mu = 0.66 \pm 0.01$ d^{-1} (Fig. 7). In the N-depleted treatment, cell growth decreased from day 7, and the same cell density was maintained until the end of culture (day 10). The growth rate of the cells in the Fe-depleted medium decreased from day 3 or 4, but cell density increased gradually at a growth rate of $\mu = 0.22 \pm 0.03$ d^{-1} until the end of the experiment (day 9) (Fig. 7). At the end of culture, the PN concentrations were 40, 11, and 10 μmol L^{-1} under the controls, N-depleted, and Fe-depleted conditions, respectively. These results suggest that macronutrients were replete in the controls throughout the course of the experiment, nitrate was exhausted under the N-depleted conditions, and severe iron-limitation reduced nitrate drawdown.

Cell quota of bioactive elements.

The carbon and nitrogen contents of the algal cells were significantly higher in the Fe-depleted treatments, compared with the N-depleted treatments and the controls (Fig 8a, 8b). Si cell quota differed significantly between treatments, with the highest amounts found in the N-depleted treatments, followed by the Fe-depleted treatments and the controls (Fig 8c). The chlorophyll-*a* cell quota was significantly higher in the controls compared with the N- and Fe-depleted treatments (Fig 8d). There were no significant differences in the carbon to nitrogen ratio among the treatments (6.5 ± 0.8 for the control, 6.8 ± 0.8 for the Fe-depleted, and 8.2 ± 0.9 for the N-depleted treatment), but there were significant differences in the silicon to carbon (Si:C), and silicon to nitrogen (Si:N) ratios. Si:C and Si:N ratios were highest for cells cultured in the N-depleted media (Si:C: 0.80 ± 0.10, Si:N: 6.5 ± 0.4), followed by cells from the Fe-depleted treatments (Si:C: 0.46 ± 0.02, Si:N: 3.1 ± 0.5) and the controls (Si:C: 0.28 ± 0.03, Si:N: 1.8 ± 0.4).

Cell geometry.

Cells from the controls had significantly greater surface areas (SA) and cell volumes (CV), than those from the N- and Fe-depleted treatments (Fig. 9a, 9b). The smaller cell volume and surface area of cells grown in the N- and Fe-depleted media were mainly due to a reduction in cell height (controls: 15.8–31.5 μm, N-depleted: 10.9–21.3 μm, Fe-depleted: 5.0–14.3 μm).

In contrast, horn length was significantly greater in the algal cells cultured under Fe-depleted conditions (52.2–67.8 μm), compared with those in the N-depleted treatment (35.6–56.5 μm) and the controls (33.8–47.9 μm) (Figs 4–6 and 9c). The SA/CV ratios were significantly higher in cells from the Fe-depleted treatment, followed by the N-depleted treatment and the controls (Fig. 4d).

Estimated sinking rate.

To estimate the cell sinking rates applying Stokes' law, constant values were used for all the parameters (ρ_{sw} = 1025 kg m^{-3} and η = 0.00151 kg m^{-1} s^{-1}; Peperzak et al. 2003) except cell radius and particulate density. Assuming that excess cell density relative to that of seawater was derived solely from the Si content (Sommer 1988), the excess density (i.e., $\rho_p - \rho_{sw}$ in eq. 1) of vegetative cells in the control would be 75 kg m^{-3} (i.e., ρ_p = 1100 kg m^{-3}; Peperzak et al. 2003, Si content of 0.28 pmol $cell^{-1}$). That of N-depleted cells would be 206 kg m^{-3} (0.77 pmol Si $cell^{-1}$) and 174 kg m^{-3} (0.65 pmol Si $cell^{-1}$) for Fe-depleted cells. The estimated sinking rate was fastest under the N-depleted conditions (Fig. 9e), as this treatment showed the highest Si content. The estimated sinking rate of the cells with prolonged horns and a more than 2-fold increase in Si quota under Fe-depleted conditions was slower than that under the controls (Fig. 9e).

Discussion

This study shows that *A. longicornis* could reduce its estimated sinking rate with a simultaneous increase in horn length, SA/CV ratio and Si cell quota under Fe-depleted conditions. These results support previous assumptions that the spines of *Chaetoceros* species may improve the regulation of sinking rate relative to that attainable by spine-free cells (Timmermans et al. 2001, Raven & Waite 2004). Sugie & Kuma (2008) and Sugie & Yoshimura (2013) also showed an increase in the SA/CV ratio of the diatoms *Thalassiosira nordenskioeldii* and *Pseudo-nitzschia pseudodelicatissima* under Fe-depleted/limited conditions. However, the actual sinking rate of Fe-depleted *T. nordenskioeldii* resting cells and resting spores was about twice as fast as that of vegetative cells (Sugie & Kuma 2008). The difference in the SA/CV ratio between the vegetative and Fe-depleted cylindrical *T.*

291 *nordenskioeldii* cells was small (approximately 25%), compared with the difference in *A.*
292 *longicornis*, with its finely structured horns (128%). Turbulent mixing is a key factor
293 regulating the sinking behaviour of particles in the ocean (e.g. Margalef 1997, Huisman et al.
294 2002). Increasing the surface area to volume ratio increases the physical resistance between
295 the cell surface and the water. For diatoms to actively regulate their sinking rate, substantial
296 respiratory energy would be required (Waite et al. 1992). Iron-limitation depresses
297 photosynthesis and therefore limits the energy available for respiration (Muggli et al. 1996).
298 However, silicon uptake may be independent of iron-requiring processes, and silicification
299 requires less energy than the formation of cellulose cell walls (Martin-Jézéquel et al. 2000).
300 Elongation of siliceous horns under Fe-depleted and respiratory energy-limited conditions
301 may be an ideal adaptive strategy to regulate the sinking rates in the open ocean.
302 In previous studies, *A. longicornis* was often found in the iron-limited open subarctic
303 Pacific Ocean during spring and summer (Sugie et al. 2010a). As Fe-limited regions are
304 generally located in the open ocean (Moor et al. 2013), where the seafloor is permanently
305 aphotic, a slow sinking rate under Fe-limited conditions should increase the rate of survival.
306 In some Fe-limited regions such as the western subarctic gyre, chain-forming diatoms are
307 usually scarce (Tsuda et al. 2005, Sugie & Suzuki in press). Micronutrient-limitation induces
308 resting stages in coastal chain-forming species, which have fast sinking rates (Sugie & Kuma
309 2008, Sugie et al. 2010a). Under iron-limited conditions, the long horns of *A. longicornis* could
310 act to increase the SA/CV ratio, rather than entanglement with the *Chaetoceros* chain. Small
311 cell size can be beneficial for the uptake of limiting nutrient due to a small diffusive boundary
312 layer (Pahlow et al. 1997, Raven 1998). In addition, small-celled species can assimilate
313 nutrients more efficiently than large-celled species (Raven 1998, Raven & Waite 2004). The
314 low chlorophyll-*a* content of *A. longicornis* cells under Fe-depleted conditions could also
315 reduce cellular photo-oxidative damages in sunlit surface waters during summer, as suggested
316 previously (Sugie et al. 2011).
317 Nitrogen is a primary limiting nutrient in the coastal region, where phytoplankton can
318 exhaust nitrate under high iron availability (Tyrrell & Law 1997, Sugie et al. 2010b). Under
319 N-depleted conditions, heavily silicified *A. longicornis* may have a faster sinking rate and

320 therefore tended to sink to deeper waters. Coastal diatoms often form resting stages under
321 macronutrient-depleted conditions, which is an ecological strategy to sink faster in the neritic
322 regions, to avoid grazing by zooplankton and photo-oxidative stresses in the nutrient-depleted,
323 sunlit surface waters (Hargraves & French 1983, Smetacek 1985, Sugie & Kuma 2008, Sugie
324 et al. 2010a). Diatoms surviving on the neritic seafloor can return to the surface layer via
325 mixing events and increase populations under the favourable growth conditions. Although we
326 did not observe the resting spores of *A. longicornis* under the N-depleted conditions, previous
327 reports suggest that the resting cells of this species could survive at least several months on
328 the seafloor (McQuoid 2005, Tsukazaki et al. 2013).
329 The insignificant change in the cellular C:N ratio under the N- and Fe-depleted
330 conditions indicates that the intracellular carbon and nitrogen metabolism are tightly coupled.
331 According for the change in cell size, compared to the controls the intracellular carbon and
332 nitrogen concentrations increased about 2- and 5-fold under the N- and Fe-depleted conditions,
333 respectively. Although the possible mechanisms for high intracellular N concentrations remain
334 uncertain, *A. longicornis* may store nutrients under unfavourable growth conditions. Unlike
335 the increase in *A. longicornis*, Fe-limitation generally decreases the cellular nitrogen content
336 of diatoms such as *Pseudo-nitzschia* spp. (e.g. Marchetti & Cassar 2009, Sugie & Yoshimura
337 2013). In previous studies under N-limited conditions, the C:N ratio increased because of a
338 large increase in C content, whereas the N content remained constant, or was only slightly
339 higher than in vegetative cells (French & Hargraves 1980, Kuwata et al. 1993). This suggests
340 that the relatively small change in C content under N- and Fe-depleted conditions in *A.*
341 *longicornis* is unique and may contribute to the stable cellular C:N ratio under different growth
342 conditions. In contrast, Si:C and Si:N ratios increased under both the N- and Fe-depleted
343 conditions. The higher Si cell quota with a smaller SA under N- and Fe-depleted conditions
344 indicates that *A. longicornis* is more heavily silicified under the unfavourable growth
345 conditions than control conditions. Longer horns under Fe-depletion may contribute to the
346 higher Si content compared with the controls. An increase in the Si:N and Si:C ratios in
347 diatoms grown under an N- or Fe-limited/depleted conditions is well-known (French &
348 Hargraves 1980, Kuwata et al. 1993, Marchetti & Cassar 2009, Sugie et al. 2010a, Sugie &

Yoshimura 2013). Diatoms increase the Si:C and Si:N ratios in two ways; Type-1 increases silicification, e.g. *Actinocyclus* sp., *Chaetoceros pseudocurvisetus* and *Thalassiosira nordenskioeldii*, (Kuwata et al. 1993, Timmermans et al. 2004, Sugie et al. 2010a) and Type-2 decreases cellular C and N content, e.g. *Chaetoceros dichaeta*, and *Pseudo-nitzschia* spp., (Takeda 1998, Marchetti & Cassar 2009, Sugie & Yoshimura 2013). *Attheya longicornis* is a Type-1 species under both N- and Fe-depleted conditions. These results suggest that *A. longicornis* took up dissolved silicic acid from ambient seawater after both N and Fe were depleted. Similar over-consumption of Si compared to N uptake under N- and Fe-depletion has been reported previously from the natural phytoplankton community in the Oyashio region during the spring diatom bloom (Sugie et al. 2010a). However, the different estimated sinking behaviour of *A. longicornis* under the N- and Fe-depleted conditions could result in biogeochemical cycling of Si in opposite directions; the former might sequester Si in deeper waters, whereas the latter might retain Si in the surface.

***Insights into the autecology of* A. longicornis**

Diatom biogeography in the open ocean is strongly affected by current systems originating from coastal regions where species are abundant, with species-specific ecological traits modifying the subsequent distribution patterns (Sugie & Suzuki in press). *Attheya longicornis* is often found in the subarctic seas in the coastal region, tangled by its hon with chain-forming diatoms by its horns (Orlova et al. 2002, Stonik et al. 2006), which significantly increases particle size. Because grazing pressure decreases with increasing cell size (Thingstad et al. 2005), entanglement with, or attachment to a large cell or chain by small species could decrease the grazing pressure by zooplankton. Many chain-forming diatoms are coastal species, such as *Chaetoceros* subgenus *Hyalochaete* (Smetacek 1985, Round et al. 1990, Sugie et al. 2010a) and chain formation may allow diatoms to live as plankton only under high nutrient and turbulent conditions based on nutrient uptake models (Pahlow et al. 1997). After either macro- or micronutrient depletion, such large chain-forming diatoms would decrease their abundance partly due to the formation of fast-sinking resting spores (Smetacek 1985, Sugie & Kuma 2008). *Attheya longicornis* increased its Si quota under Fe- and N-depleted conditions, but the probable fate of biogenic Si may differ depending on the sinking behaviour.

To sustain the local population of *A. longicornis* under unfavourable growth conditions, a change in sinking behaviour appears to be beneficial, both in the coastal and open ocean of the subarctic. Such physiological plasticity may contribute to their wide distribution in these regions (Orlova et al. 2002, Stonik et al. 2006, Sugie et al. 2010a, Malviya et al. 2016, Sugie and Suzuki in press). These suggested ecophysiological strategies of diatoms with spiny siliceous structures need additional study, but the available data suggest that the *A. longicornis* increases its survival rate by altering its ecological strategies depending on the nutrient-limiting conditions.

Acknowledgements

It is grateful that invaluable comments from two anonymous reviewers significantly improved this manuscript. This work was supported by grants from the Sasakawa Scientific Research Grant from the Japan Science Society to K. S., for Scientific Research Project from the Research Institute for Humanity and Nature to K. K., and for Scientific Research (18201001) from the Ministry of Education, Culture, Sports, Science and Technology to K. K. The SEM analysis of *A. longicornis* frustules were carried out with JSM-6360LA at the OPEN FACILITY, Hokkaido University Sousei Hall.

References

Boyd P.W., Jickells T., Law C.S., Blain S., Boyle E.A., Buesseler K.O., Coale K.H., Cullen J.J., de Baar H.J.W., Follows M., Harvey M., Lancelot C., Levasseur M., Owens N.P.J., Pollard R., Rivkin R.B., Sarmient J., Schoemann V., Smetacek V., Takeda S., Tsuda A., Turner S., Watson A.J. 2007. Mesoscale iron enrichment experiments 1993–2005: Synthesis and future directions. *Science* 315: 612–616.

Brzezinski M.A. & Nelson D.M. 1988. Differential cell sinking as a factor influencing diatom species competition for limiting nutrients. *Journal of Experimental Marine Biology and Ecology* 119: 179–200.

Brzezinski M.A., Pride C.J., Frank V.M., Sigman D.M., Sarmiento J.L., Matsumoto K., Gruber N., Rau G.H. & Coale K.H. 2002. A switch from $Si(OH)_4$ to NO_3^- depletion in the glacial

Southern Ocean. *Geophysical Research Letters* 29: 12, doi:10.1029/2001GL014349.

Crawford R.M., Gardner C. & Medlin L.K. 1994. The genus *Attheya*. I. A description of four new taxa, and the transfer of *Gonioceros septentrionalis* and *G. armatas*. *Diatom Research* 9: 27–51.

Crawford R.M. 1995. The role of sex in the sedimentation of a marine diatom bloom. *Limnology and Oceanography* 40: 200–204.

De La Rocha C., Nowald N. & Passow U. 2008. Interactions between diatom aggregates, minerals, particulate organic carbon, and dissolved organic matter: Further implications for the ballast hypothesis. *Global Biogeochemical Cycles* 22: GB4005, doi:10.1029/2007GB003156.

Falkowski P.G., Barber R.T. & Smetacek V. 1998. Biogeochemical control and feedbacks on ocean primary production. *Science* 281: 200–206.

French F.W. & Hargraves P.E. 1980. Physiological characteristics of plankton diatom resting spores. *Marine Biology Letters* 1: 185–195.

Guillard R.R.L. & Ryther J.H. 1962. Studies of marine planktonic diatoms. I. *Cyclotella nana* Hustedt and *Detonula confervacea* (Gleve) Gran. *Canadian Journal of Microbiology* 8: 229–239.

Hargraves P.E. & French F.W. 1983. Diatom resting spores: significance and strategies. In: *Survival strategies of the algae* (Ed. by G.A. Fryxell), pp. 49–68. Cambridge Univ Press, New York.

Hillebrand H., Durseien C.D., Kirschtel D., Pollingher U. & Zohary T. 1999. Biovolume calculation for pelagic and benthic microalgae. *Journal of Phycology* 35: 403–424.

Huisman J., Arrayás M., Ebert U. & Sommeijer B. 2002. How do sinking phytoplankton species manage to persist? *American Naturalist* 159: 245–254.

Iwade S., Kuma K., Isoda Y., Yoshida M., Kudo I., Nishioka J. & Suzuki K. 2006. Effect of high iron concentrations on iron uptake and growth of a coastal diatom *Chaetoceros sociale*. *Aquatic Microbial Ecology* 43: 177–191.

Kuwata A., Hama T. & Takahashi M. 1993. Ecophysiological characterization of two life forms, resting spores and resting cells, of a marine planktonic diatom, *Chaetoceros*

436 *pseudocurvisetus*, formed under nutrient depletion. *Marine Ecology Progress Series* 102:
437 245–255.
438 Malviya S., Scalco E., Audic S., Vincent F., Veluchamy A., Poulain J., Wincker P., Iudicone
439 D., de Vargas C., Bittner L., Zingone A. & Bowler C. 2016. Insights into global diatom
440 distribution and diversity in the world's ocean. *Proceeding of the National Academy of*
441 *Science U.S.A.* 113: E1516-E1525. doi:10.1073/pnas.1509523113.
442 Marchetti A. & Cassar N. 2009. Diatom elemental and morphological changes in response to
443 iron limitation: a brief review with potential paleoceanographic applications. *Geobiology*
444 7: 1–13.
445 Margalef R. 1997. Turbulence and marine life. In: Lectures on plankton and turbulence. (Eds.
446 C. Marrasé, E. Saiz & J.M. Redondo), *Scientia Marina* 61: 109–123.
447 Martin-Jézéquel V., Hildebrand M. & Brzezinski M.A. 2000. Silicon metabolism in diatom:
448 implications for growth. *Journal of Phycology* 36: 821–840.
449 McQuoid M.R. 2005. Influence of salinity on seasonal germination of resting stages and
450 composition of microplankton on the Swedish west coast. *Marine Ecology Progress*
451 *Series* 289: 151–163.
452 Moor C.M., Mills M.M., Arrigo K.R., Berman-Frank I., Bopp L., Boyd P.W., Galbraith E.D.,
453 Geider R.J., Guieu C., Jaccard S.L., Jickells T.D., La Roche J., Lenton T.M., Mahowald
454 N.M., Maranon E., Marinov I., Moore J.K., Nakatsuka T., Oschlies A., Saito M.A.,
455 Thingstad T.F., Tsuda A. & Ulloa O. 2013. Processes and patterns of oceanic nutrient
456 limitation. *Nature Geoscience* 6: 701–710.
457 Morel F.M.M., Rueter J.G., Anderson D.M. & Guillard R.R.L. 1979. AQUIL: A chemically
458 defined phytoplankton culture medium for trace metal studies. *Journal of Phycology* 15:
459 135–141.
460 Muggli D.L., Lecourt M. & Harrison P.J. 1996. Effects of iron and nitrogen source on the
461 sinking rate, physiology and metal composition of an oceanic diatom from the subarctic
462 Pacific. *Marine Ecology Progress Series* 132: 215–227.
463 Nagumo T. 1995. Simple and safe cleaning methods for diatom samples. *Diatom* 10: 88 (in
464 Japanese).

Obata H., Karatani H. & Nakayama E. 1993. Automated determination of iron in seawater by chelating resin concentration and chemiluminescence detection. *Analytical Chemistry* 65: 1524–1528.

Orlova T.Y., Stonik I.V. & Aizdaicher N.A. 2002. Morphology and biology of the diatom alga *Attheya longicornis* from the Sea of Japan. *Russian Journal of Marine Biology* 28: 186–190.

Paasche E. 1980. Silicon content of five marine plankton diatom species measured with a rapid filter method. *Limnology and Oceanography* 25: 474–480.

Pahlow M., Riebesell U. & Wolf-Gladrow D.A. 1997. Impact of cell shape and chain formation on nutrient acquisition by marine diatoms. *Limnology and Oceanography* 42: 1660–1672.

Peperzak L., Colijn F., Koeman R., Gieskes W.W.C. & Joordens J.C.A. 2003. Phytoplankton sinking rates in the Rhine region of freshwater influence. *Journal of Plankton Research* 25: 365–383.

Rampen S.W., Schouten S., Panoto F.E., Brink M., Anderson R.A., Muyzer G., Abbas B. & Damsté J.S.S. 2009. Phylogenic position of *Attheya longicornis* and *Attheya septentrionalis* (Bacillariophyta). *Journal of Phycology* 45: 444–453.

Raven J.A. 1998. Small is beautiful: the picophytoplankton. *Functional Ecology* 12: 503–13

Raven J.A. & Waite A.M. 2004. The evolution of silicification in diatoms: inescapable sinking and sinking as escape? *New Phytologist* 162: 45–61.

Redfield A.C., Ketchum B.H. & Richards F.A. 1963. The influence of organisms on the composition of seawater. In: *The Sea Vol. 2* (Ed. N.M. Hill), pp. 26–77. Wiley, New York.

Round, F.E., Crawfrod, R.M. & Mann, D.G. 1990. *The Diatoms. Biology and morphology of the genera*. Cambridge University Press, Cambridge. pp. 747.

Sommer U. 1988. Growth and survival strategies of planktonic diatoms. In: *Growth and reproductive strategies of freshwater phytoplankton* (Ed. C.D. Sandgren), pp. 227–260. Cambridge University Press, Cambridge.

Smetacek V. 1985. Role of sinking diatom life-history cycles: ecological, evolutionary and geological significance. *Marine Biology* 84: 239–251.

494 Smetacek V. 1999. Diatoms and the ocean carbon cycles. *Protist* 150: 25–32.
495 Smetacek V. 2001. A watery arms race. *Nature* 411:745–745.
496 Stonik I.V., Orlova T.Y. & Aizdaicher N.A. 2006. Diatoms of the genus *Attheya* West, 1860
497 from the Sea of Japan. *Russian Journal of Marine Biology* 32: 123–126.
498 Sugie K. & Kuma K. 2008. Resting spore formation in the marine diatom *Thalassiosira*
499 *nordenskioeldii* under iron- and nitrogen-limited conditions. *Journal of Plankton*
500 *Research* 30: 1245–1255.
501 Sugie K., Kuma K., Fujita S. & Ikeda T. 2010a. Increase in Si:N drawdown ratio due to resting
502 spore formation by spring bloom-forming diatoms under Fe- and N-limited condition in
503 the Oyashio region. *Journal of Experimental Marine Biology and Ecology* 382: 108–116.
504 Sugie K., Kuma K., Fujita S., Nakayama Y., Ikeda T. 2010b. Nutrient and diatom dynamics
505 during late winter and spring in the Oyashio region of the western subarctic Pacific Ocean.
506 *Deep-Sea Research* II 57: 1630–1642.
507 Sugie K., Kuma K., Fujita S., Ushizaka S., Suzuki K. & Ikeda T. 2011. Importance of
508 intracellular Fe pools on growth of marine diatoms by using unialgal cultures and the
509 Oyashio region phytoplankton community during spring. *Journal of Oceanography* 67:
510 183–196.
511 Sugie K. & Yoshimura T. 2013. Effects of pCO_2 and iron on the elemental composition and
512 cell geometry of the marine diatom *Pseudo-nitzschia pseudodelicatissima*
513 (Bacillariophyceae). *Journal of Phycology* 49: 475–488.
514 Sugie K. & Suzuki K. in press. Characterization of the synoptic-scale diversity, biogeography
515 and size distribution of diatoms in the North Pacific. *Limnology and Oceanography*:
516 doi:10.1002/lno10473.
517 Suzuki R. & Ishimaru T. 1990. An improved method for the determination of phytoplankton
518 chlorophyll using N, N-dimethylformamide. *Journal of the Oceanographic Society of*
519 *Japan* 46: 190–194.
520 Takeda S. 1998. Influence of iron availability on nutrient consumption ratio of diatoms in
521 oceanic waters. *Nature* 393: 774–777.
522 Thingstad T.F., Øvreås L., Egge J.K., Løvdal T. & Heldal M. 2005. Use of non-limiting

523 substrates to increase size; a generic strategy to simultaneously optimize uptake and
524 minimize predation in pelagic osmotrophs? *Ecology Letters* 8: 675–682.
525 Timmermans K.R., Davey M.S., van der Wagt B., Snoek J., Geider R.J., Veldhuis M.J.W.,
526 Gerringa L.J.A. & de Baar H.J.W. 2001. Co-limitation by iron and light of *Chaetoceros*
527 *brevis*, *C. dichaeta* and *C. calcitrans* (Bacillariophyceae). *Marine Ecology Progress*
528 *Series* 217: 287–297.
529 Timmermans K.R., van der Wagt B. & de Baar H.J.W. 2004. Growth rates, half-saturation
530 constants, and silicate, nitrate, and phosphate depletion in relation to iron availability of
531 four large, open-ocean diatoms from the Southern Ocean. *Limnology and Oceanography*
532 49: 2141–2151.
533 Tsuda A., Kiyosawa H., Kuwata A., Mochizuki M., Shiga N., Saito H., Chiba S., Imai K.,
534 Nishioka J. & Ono T. 2005. Responses of diatoms to iron-enrichment (SEEDS) in the
535 western subarctic Pacific, temporal and spatial comparisons. *Progress in Oceanography*
536 64: 189–205.
537 Tsukazaki C., Ishii K., Saito R., Matsuno K., Yamaguchi A. & Imai I. 2013. Distribution of
538 viable diatom resting stage cells in bottom sediments of the eastern Bering Sea shelf.
539 *Deep-Sea Research II* 94: 22–30.
540 Tyrrell T. & Law S. 1997. Low nitrate : phosphate ratios in the global ocean. *Nature* 387: 793–
541 796.
542 Waite A.M., Thompson P.A. & Harrison P.J. 1992. Does energy control the sinking rates of
543 marine diatoms? *Limnology and Oceanography* 37: 468–477.
544 Weber T.S. & Deutsch C. 2010. Ocean nutrient ratios governed by plankton biogeography.
545 *Nature* 467: 550–554.
546 Welschmeyer N.A. 1994. Fluorometric analysis of chlorophyll *a* in the present of chlorophyll
547 *b* and pheopigments. *Limnology and Oceanography* 39: 1985–1992.
548 Wilken S., Hoffmann B., Hersch N., Kirchgessner N., Dieluweit S., Rubner W., Hoffmann L.J.,
549 Merkel R. & Peeken I. 2011. Diatom frustules show increased mechanical strength and
550 altered valve morphology under iron limitation. *Limnology and Oceanography* 56: 1399–
551 1410.

Yoshida M., Kuma K., Iwade S., Isoda Y., Takata H. & Yamada M. 2006. Effect of aging time on the availability of freshly precipitated ferric hydroxide to coastal marine diatoms. *Marine Biology* 149: 379–392.

Figure captions

Figs 1–6. Images of *Attheya longicornis*. Cells attached to Fig 1. *Chaetoceros diadema* and Fig 2. *Chaetoceros socialis* (samples were collected from the Oyashio region in April 2007). Scanning electron micrograph of Fig 3. *A. longicornis* (scale bar is 5 μm), with a detailed image of a siliceous horn in the insert (scale bar is 1 μm). Cells grown under Fig 4. nutrient-replete conditions (control), Fig 5. N-depleted conditions and Fig 6. Fe-depleted conditions.

Fig. 7. Temporal change in cell density of *Attheya longicornis* grown under nutrient-replete (control), N-depleted and Fe-depleted conditions.

Fig. 8. Change in the cell quota of (a) carbon, (b) nitrogen, (c) biogenic silica and (d) chlorophyll-*a* for *Attheya longicornis* in controls and N- and Fe- depleted conditions. Alphabet above the bars indicate when the data are significantly different (Tukey's HSD test).

Fig. 9. Values for (a) cell volume, (b) surface area, (c) spine length (d) surface area to cell volume ratio and (e) estimated sinking rate of *Attheya longicornis* cells grown in nutrient-replete (control) and N- and Fe-depleted conditions. Alphabet above the bars indicate when the data are significantly different (Tukey's HSD test).

Table 1. Tree treatments examining the effect of nitrogen- and Fe-depletion on the elemental composition and morphology of *Attheya longicornis*.

Treatment	Nutrients	Iron
Control	Replete	Replete (+100 nmol L^{-1})
N-depleted	11 μmol L^{-1} NO_3 (P and Si replete)	Replete (+100 nmol L^{-1})
Fe-depleted	Replete	1 μmol L^{-1} DFB (No Fe additon)

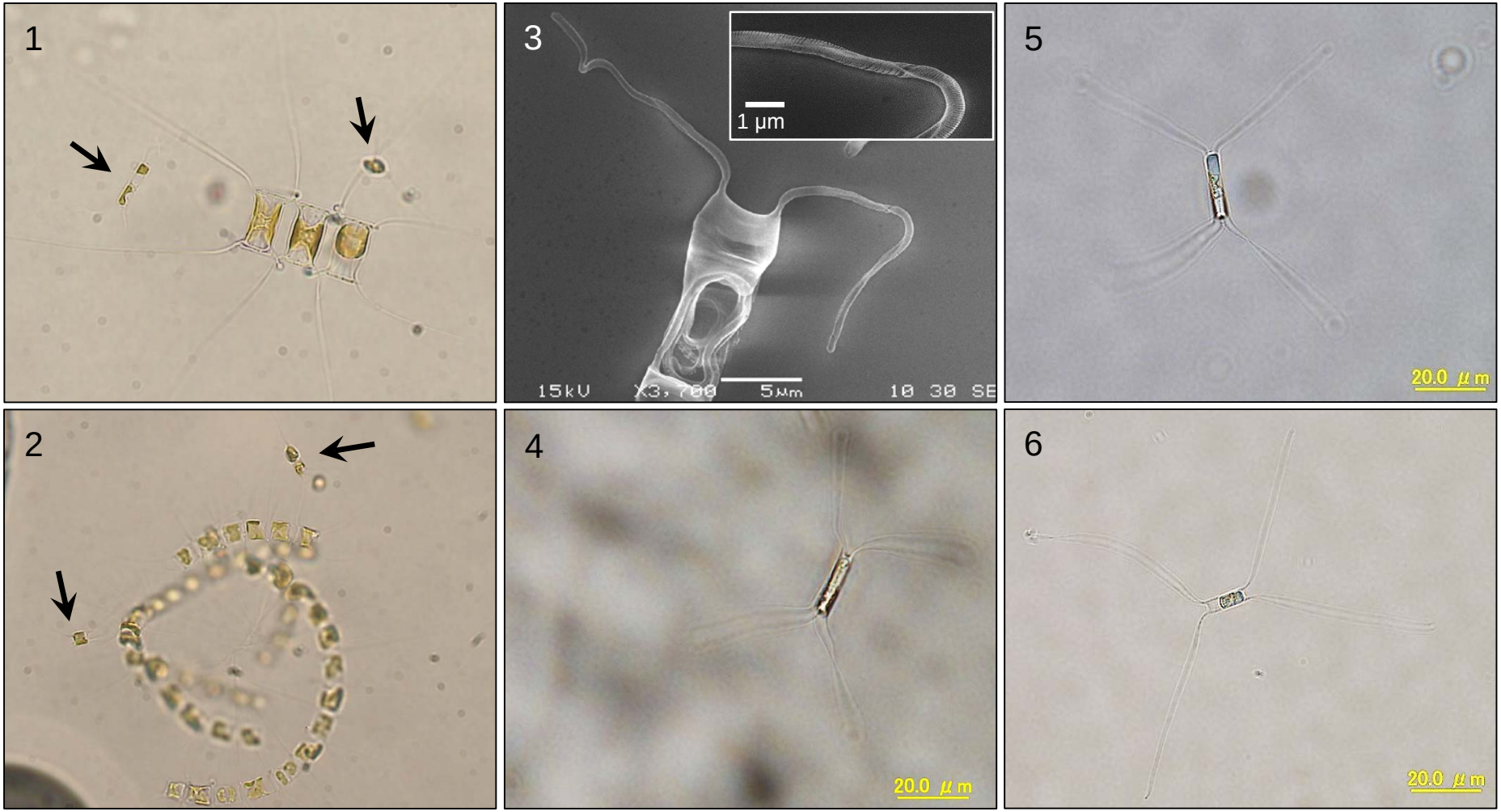
1
2
3
1 µm
15kV X3,700 5µm 10 30 SE
4
20.0 µm
5
20.0 µm
6
20.0 µm

Fig. 7

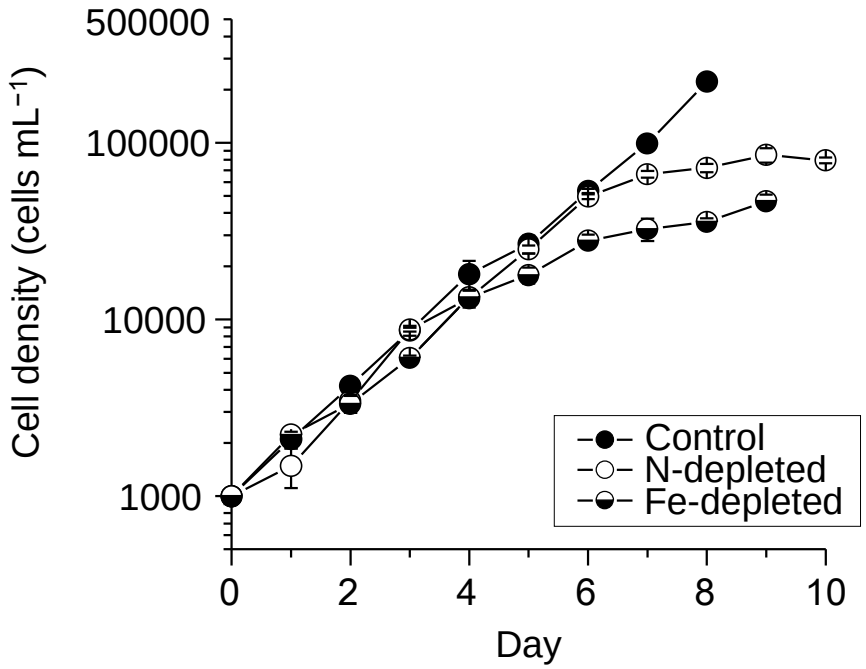
500000
100000
10000
1000
Cell density (cells mL^{-1})
0
2
4
6
8
10
Day
Control
N-depleted
Fe-depleted

Fig. 8

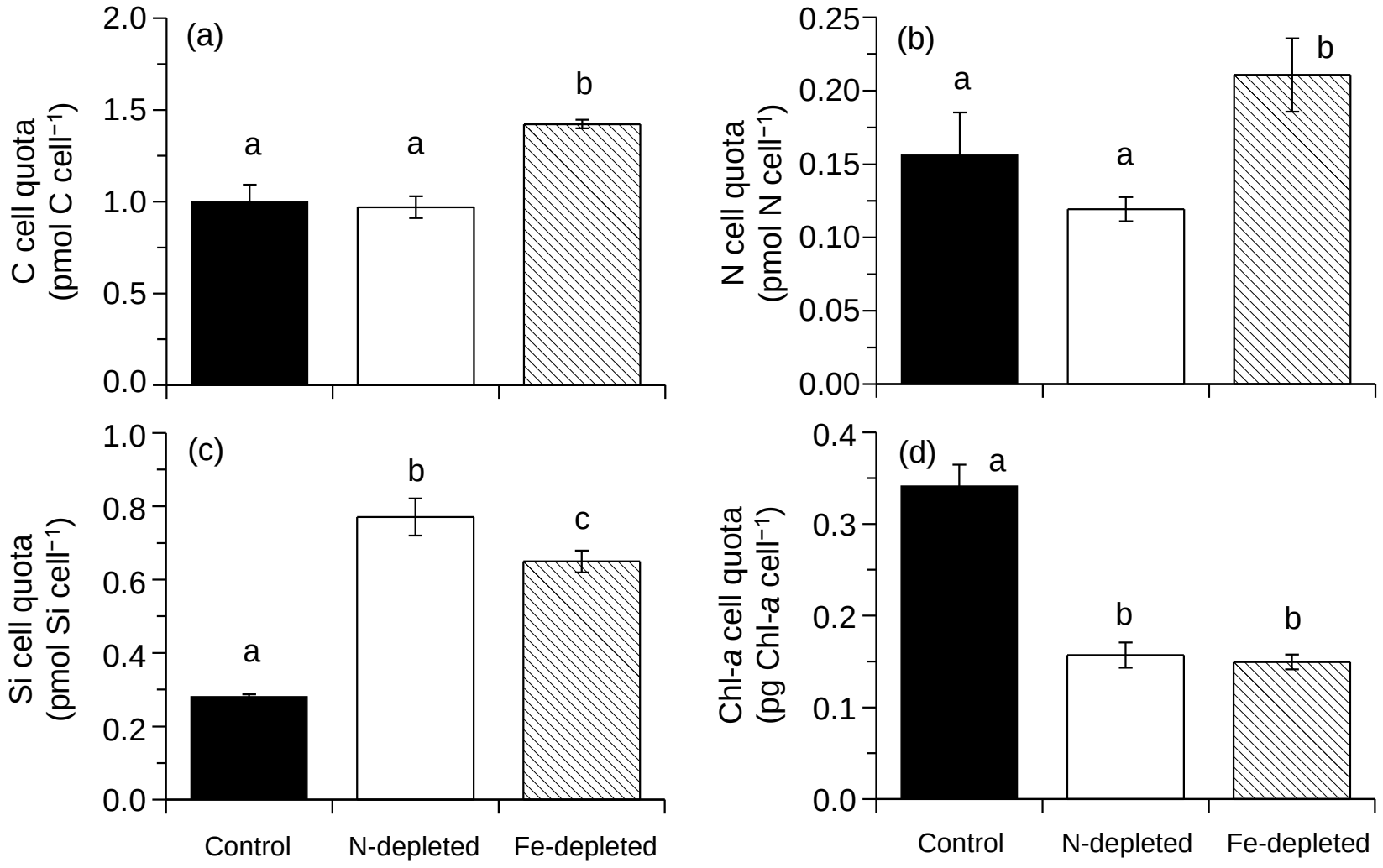
(a)
C cell quota (pmol C cell⁻¹)
2.0
1.5
1.0
0.5
0.0
a
a
b
(b)
N cell quota (pmol N cell⁻¹)
0.25
0.20
0.15
0.10
0.05
0.00
a
a
b
(c)
Si cell quota (pmol Si cell⁻¹)
1.0
0.8
0.6
0.4
0.2
0.0
a
b
c
(d)
Chl-a cell quota (pg Chl-a cell⁻¹)
0.4
0.3
0.2
0.1
0.0
a
b
b
Control
N-depleted
Fe-depleted
Control
N-depleted
Fe-depleted

Fig. 9

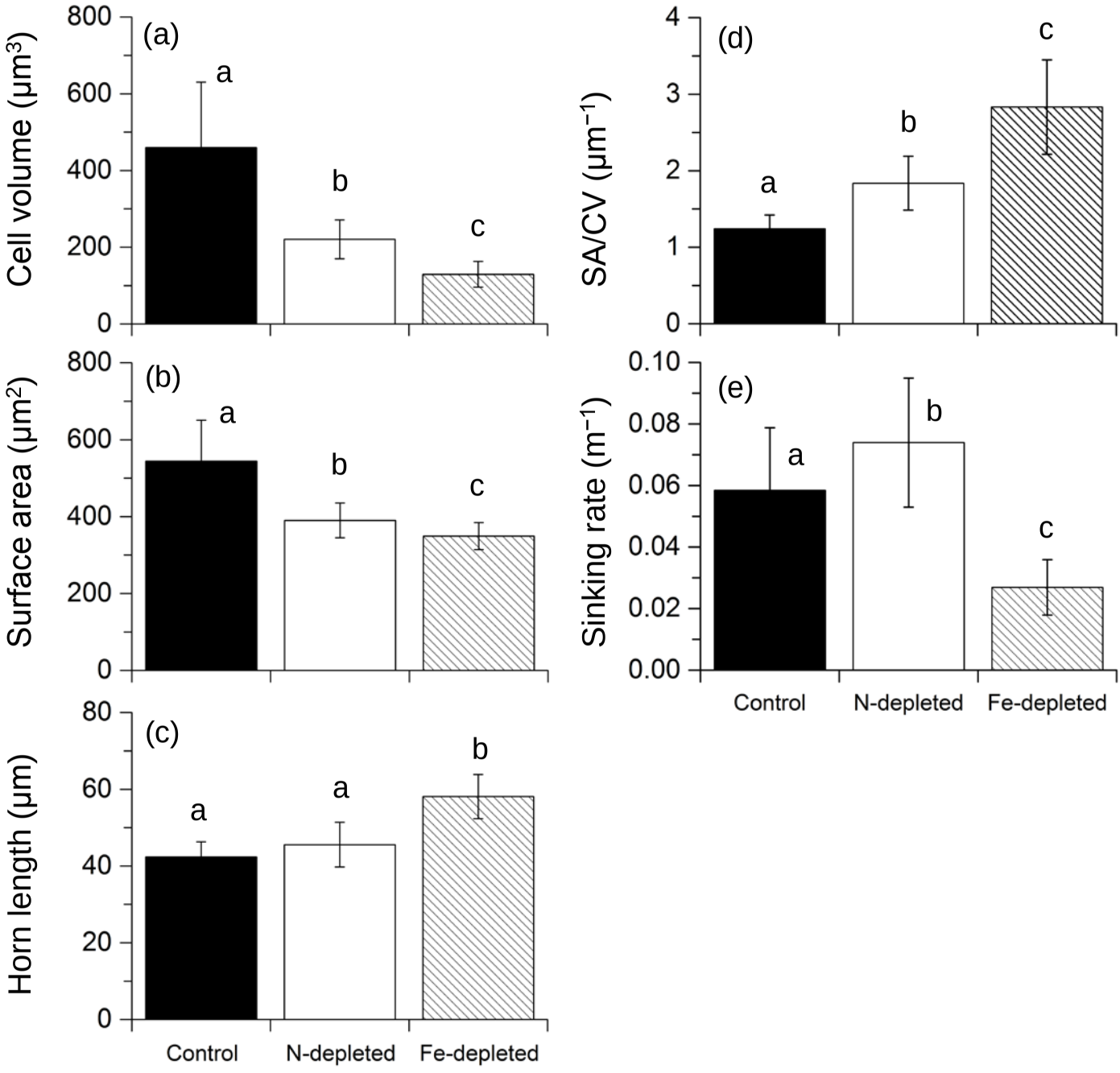
(a)
Cell volume (µm³)
800
600
400
200
0
a
b
c
(b)
Surface area (µm²)
800
600
400
200
0
a
b
c
(c)
Horn length (µm)
80
60
40
20
0
a
a
b
Control
N-depleted
Fe-depleted
(d)
SA/CV (µm⁻¹)
4
3
2
1
0
a
b
c
(e)
Sinking rate (m⁻¹)
0.10
0.08
0.06
0.04
0.02
0.00
a
b
c
Control
N-depleted
Fe-depleted